Hints for a General Understanding of the Epitaxial Rules for van der Waals Epitaxy from Ge-Sb-Te Alloys

Fabrizio Arciprete,* Jos Emiel Boschker, Stefano Cecchi,* Eugenio Zallo, Valeria Bragaglia, and Raffaella Calarco

In this study, a generalized guideline is identified to predict the interaction between two-dimensional (2D) layered materials and substrate surfaces. Additionally, the van der Waals (vdW) heterostructures commensurability, the phase formation and the strain relaxation are identified during interface growth. To achieve such a general overview, the case of Ge-Sb-Te (GST) alloys on InAs(111) is studied. In this system, low-lattice mismatch conditions are fulfilled to avoid relaxation due to formation of misfit dislocations and allow to correctly identify vdW epitaxy. At the same time, the substrate can be efficiently prepared into self- and un-passivated surfaces to clarify the role of the surface interaction. Furthermore, the GST epilayer exhibits two different highly ordered 2D structures and a three-dimensional disordered structure, allowing to directly infer the nature of the epitaxy. This study opens the way for the design and mastering of vdW epitaxial growth of 2D heterostructures as well as hybrid 2D and non-layered materials.

F. Arciprete, J. E. Boschker,[+] S. Cecchi,[++] E. Zallo,[+++] V. Bragaglia,[++++]
R. Calarco
Paul-Drude-Institut für Festkörperelektronik
Leibniz-Institut im Forschungsverbund Berlin e.V.
Hausvogteiplatz 5–7, 10117 Berlin, Germany
E-mail: cecchi@pdi-berlin.de
F. Arciprete
Dipartimento di Fisica
Università di Roma "Tor Vergata"
Via della Ricerca Scientifica 1, Rome 00133, Italy
E-mail: fabrizio.arciprete@roma2.infn.it
R. Calarco
Istituto per la Microelettronica e Microsistemi (IMM)
Consiglio Nazionale delle Ricerche (CNR)
Via del Fosso del Cavaliere 100, Rome 00133, Italy

[+]Present address: Ferdinand-Braun-Institut gGmbH Leibniz-Institut für Höchstfrequenztechnik, Gustav-Kirchhoff-Str. 4, 12489 Berlin, Germany

[++]Present address: Department of Materials Science University of Milano-Bicocca via R., Cozzi 55, Milano 20125, Italy

[+++]Present address: Walter Schottky Institut and Physik Department, Technische Universität München, Am Coulombwall 4, 85748 Garching, Germany

[++++]Present address: IBM Research – Zürich, Säumerstrasse 4, Rüschlikon CH–8803, Switzerland

1. Introduction

The capability of growing high-quality heteroepitaxial films of cutting-edge crystalline materials, such as two-dimensional (2D) materials, is a prerequisite for the development of forefront technological applications. 2D materials (and their heterostructures) are stacked structures that involve weak van der Waals (vdW) interactions between adjacent blocks and strong covalent bonding within each block. This feature opens up to the possibility of isolating 2D crystal sheets to be used as building blocks to create stacked sequences of 2D crystals called vdW heterostructures that show novel properties and exotic physical phenomenon.[1,2] vdW heterostructures pave the way for a broad range of applications in electronics, optoelectronics, flexible devices, sensors, and photovoltaics.[3–5] However, the route toward industrial implementation imposes the development of large-scale deposition, implying mastering vdW epitaxial growth.[6] Despite the renewed interest and intense research efforts of the last few years,[7] a general description and a complete comprehension of vdW epitaxy would help to quickly address many issues. For instance, when using graphene or other 2D crystals as buffer layers, for vdW epitaxy the underlying substrates may still interact with the growing film.[8–15] An intermediate behavior in the growth between 2D and 3D materials has also been observed, actually allowing strain engineering in these materials.[16–21] Epitaxial rules for 2D materials are therefore highly desirable to allow the prediction of substrate surface interaction, vdW heterostructures commensurability, and strain relaxation during interface growth. The formation of the vdW gaps is a fundamental feature that determines the behavior of a 2D material.[22] In this regard, the electronic properties and the morphology of the substrate surface play a key role at the very early stages of the film growth. The formation of bonds between the growing film and the substrate can occur on dangling bonds and on defects,[13,23] as well as at kinks and step edges preventing the formation of vdW gaps and determining the accumulation of strain.[16] Different symmetries between the substrate and the epilayer can also induce a certain amount of strain.[24] Hence, if the deposited 2D material is not fully relaxed, vdW epitaxy has not occurred.

In order to contribute to a general description of the vdW epitaxy, here we investigated an exemplary case based on chalcogenide $(GeTe)_m(Sb_2Te_3)_n$ alloys (Ge-Sb-Te or GST) on InAs(111). GST is a key phase change material (PCM), widely studied for its cutting-edge technological applications. It is a prominent

material for phase change memories,[25] a mature technology manufactured on a foundry basis in the past 15–20 years.[26,27] Very recently, it has attracted new interest as the most advanced emerging non-volatile memory technology for neuromorphic applications.[28–30] Depending on n and m, prototypical GST can have various compositions along the pseudobinary tie line between the 3D material GeTe and the 2D material Sb_2Te_3. The latter exhibits a sequence of quintuple layer (QL) blocks along the [111] direction intercalated by vdW gaps. Crystalline GST exhibits a metastable cubic rocksalt structure, with intrinsic vacancies randomly distributed in the Ge/Sb sublattice,[31] and an ordered cubic structure where the vacancies are organized in vacancy layers (VLs) along the [111] direction. When the VLs are completely depleted, GST undergoes a transition to a stable trigonal phase, with vdW gaps intercalating blocks of different sizes (number of layers) depending on composition: 7 for $Ge_1Sb_2Te_4$ ($m = 1$, $n = 1$), 9 for $Ge_2Sb_2Te_5$ ($m = 2$, $n = 1$) and 11 for $Ge_3Sb_2Te_6$ ($m = 3$, $n = 1$).[32] A real vdW epitaxy has been successfully demonstrated, despite the high lattice mismatch, between the 2D chalcogenide Sb_2Te_3 and passivated (no empty or half-filled dangling bonds) Si(111) substrates,[33] while coincident lattices are formed with un-passivated reconstructed Si(111) surfaces. vdW epitaxy has also been obtained for other chalcogenides, even for highly mismatched interfaces, like, e.g., $ZrTe_2$/InAs(111)[34] or $MoSe_2$/GaAs.[35] However, in the case of high-lattice mismatch, the epilayer usually relaxes quickly also for conventional materials by the formation of misfit dislocations. This can hamper the possibility to discriminate vdW epitaxy, which is typically detected by probing whether the growing layer relaxes immediately. Therefore, to be able to correctly identify vdW epitaxy, to study low-lattice mismatch conditions is necessary. This is the case of the growth of GST on InAs(111) studied here. Furthermore, InAs(111) surfaces can be efficiently passivated allowing the understanding of the role of the surface quality as well as of different surface reconstructions, self-passivated and un-passivated. In addition, the fact that GST alloys exhibit not only a 2D highly ordered trigonal structure, but also an ordered cubic structure with VLs or a rocksalt metastable phase with no vdW gaps can help to infer the nature of the epitaxy by observing the structure of the deposited GST.

2. Results and Discussion

GST films were grown by molecular beam epitaxy (MBE) (see Experimental Section for further details) on InAs(111) substrates (lattice mismatch ≈1%) of both polarities, i.e., In- and As-terminated surfaces. MBE-grown films for memory applications demonstrated excellent electrical performances.[36,37] Four different samples were grown on three different substrate surface reconstructions: InAs(111)A-2 × 2 and InAs(111)B-2 × 2 and −1 × 1. Both 2 × 2 reconstructions are self-passivated, while the 1 × 1 is meta-stable or stabilized by surface defects, thus un-passivated (see Supporting Information). Only the 2 × 2 reconstructions would allow vdW epitaxy. Reproducing well-known literature recipes,[38–42] different surface morphologies (**Table 1**) can be obtained on the respective substrate surface reconstructions, from very flat surfaces to mixed flat/rough surfaces, as evaluated from reflection high energy electron diffraction (RHEED) patterns (Figure S1 in Supporting Information). In all the cases, the growth

Table 1. GST/InAs(111)A and B samples are listed by surface reconstruction and surface morphology (see also Experimental Section, SI, and Figure S1). Observed GST epitaxy is also reported. Another GST sample (A3) was grown on InAs(111)A surface after a partial melting and recrystallization of the substrate (see Supporting Information).

Sample	Substrate	Substrate surface reconstruction	Substrate RHEED pattern	GST epitaxy
A1	InAs(111)A	2 × 2 passivated	2D/3D streaky/ spotty	vdW
A2	InAs(111)A	2 × 2 passivated	3D spotty	Classical/partially relaxed
B1	InAs(111)B	2 × 2 passivated	2D streaky	vdW
B2	InAs(111)B	1 × 1 un-passivated	2D streaky	Classical/partially relaxed

of GST leads to the formation of a clearly 2D film. In **Figure 1**a,b, we show the exemplary case of samples A1 and B1 with the well-defined streaky RHEED patterns. We note that the RHEED pattern of GST grown on the InAs(111)B-2 × 2 surface (sample B1) displays some spots superimposed to the streaks, probably due to an excess of Te segregated at the surface. Excess Te favors vacancy ordering in GST since it leads to the formation of Sb_2Te_3-rich compositions, which intrinsically contain vdW gaps, therefore leading to the formation of ordered GST.[43] A fifth GST sample (A3) was grown on InAs(111)A surface after annealing the substrate at temperatures as high as 500 °C. At these high temperatures, the surface undergoes a partial melting and recrystallization, which gives rise to the formation of nuclei with orientations other than (111) (see Figure S2, Supporting Information). The presence of grain boundaries and twin defects can influence the epitaxy of GST on InAs, which makes this defective surface interesting in our context.

According to Koma's definition of vdW epitaxy, ultrathin heterostructures with an abrupt in terms of lattice matching and thus defect-free interface can be realized.[6] Therefore, vdW epitaxy can be ruled out for all those cases where pseudomorphic growth or only partially relaxed films are obtained. Such information, in our study, is gathered from the analysis of the reciprocal space maps (RSMs). Figure 1c–f reports the RSMs around the asymmetric InAs(224) Bragg reflection of the four samples A1, A2, B1 and B2. Two distinct spots can be observed, one, most intense, is the (224) reflection of the InAs substrate while the second weaker one corresponds to the GST film [(01.13) in the case of $Ge_2Sb_2Te_5$ ($m = 2$, $n = 1$)]. The analysis of the maps for samples A1 and B1 (Figure 1c,d) suggests that GST films are fully relaxed. We can determine the in-plane lattice parameter, which is 4.233 and 4.238 Å, for samples A1 and B1, respectively. To compare with an expected in-plane lattice parameter of 4.22 Å for $(GeTe)_m(Sb_2Te_3)_n$ alloys with $m = 1,2,3$ and $n = 1$ (GST124, GST225 and GST326).[32] For sample A2 (Figure 1e), GST is partially relaxed and its final in-plane lattice parameter is 4.274 Å. For sample B2 (Figure 1f) GST and InAs peaks are aligned at the same in-plane transferred momentum Q_y almost superimposed (same in-plane lattice parameter), indicating that GST is growing pseudomorphically on InAs. In the case of sample A3 (not shown, see Supporting Information), GST and InAs peaks are almost superimposed (same lattice parameter) again indicating pseudomorphic growth.
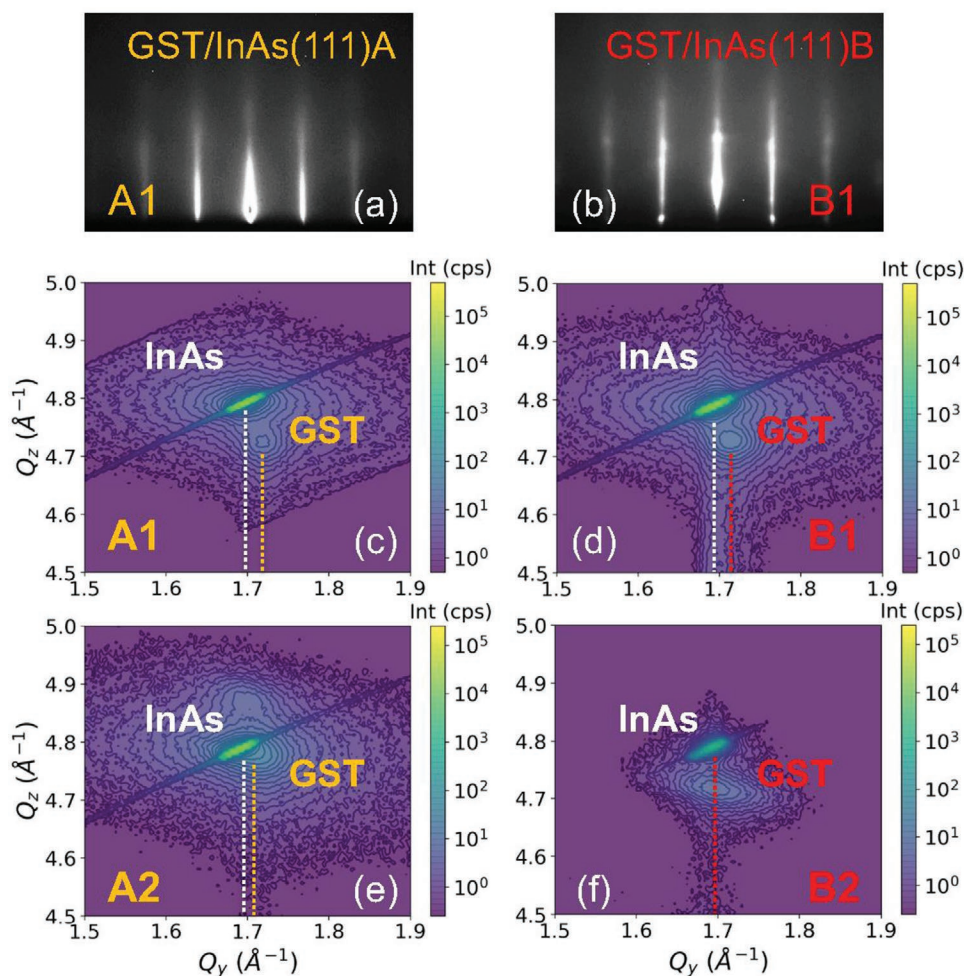
2101556 (2 of 8)

Figure 1. a,b) RHEED patterns of samples A1 and B1 acquired along ⟨1$\bar{1}$0⟩ azimuth; c–f) RSM around the asymmetric InAs(224) Bragg peak in coplanar configuration of samples A1, A2, B1 and B2.

InAs(111)B-2×2 and InAs(111)A-2×2 surfaces are self-passivated and, given the high quality of the RHEED pattern of sample B1, we expect it to be the best candidate to observe vdW epitaxy of GST. Indeed, the analysis of the in situ RHEED monitoring performed during the film growth provides a confirmation. The evolution of the in-plane lattice spacing along the [1$\bar{1}$0] direction is reported in **Figure 2** as a function of the thickness (growth rate $r_{GST} = 0.233$ nm min^{-1}) for the first 20 nm of film growth. It is possible to observe that the GST in-plane lattice parameter undergoes a fast decrease at the beginning of film growth and then a slower reduction toward the final relaxed lattice parameter (red horizontal line in Figure 2) when the GST thickness is about 5 nm, a value larger than a GST block thickness (that is in the range 1.4–2.1 nm for GST compositions from 124 to 326). In an ideal vdW epitaxy, we would expect a sharp change of the in-plane lattice parameter to the relaxed one, as indeed observed after the growth of Sb_2Te_3 on passivated Si(111) substrates.[33] Seemingly, we are observing a vdW epitaxy where the relaxation of the in-plane lattice parameter is slowing down during the growth, while it is expected that the formation of vdW gaps should speed up the relaxation. This point will be discussed below.

RSM and RHEED results suggest that vdW epitaxy may have occurred on sample B1, as expected, since the starting surface
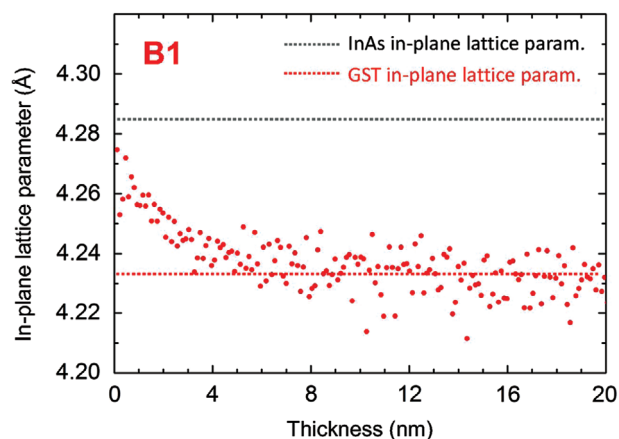

Figure 2. In-plane lattice parameter of sample B1 calculated from RHEED streak spacing along ⟨1$\bar{1}$0⟩ azimuth showing the strain relaxation during growth. Black and red dotted lines represent the in-plane lattice parameters of InAs(111) and GST, respectively.
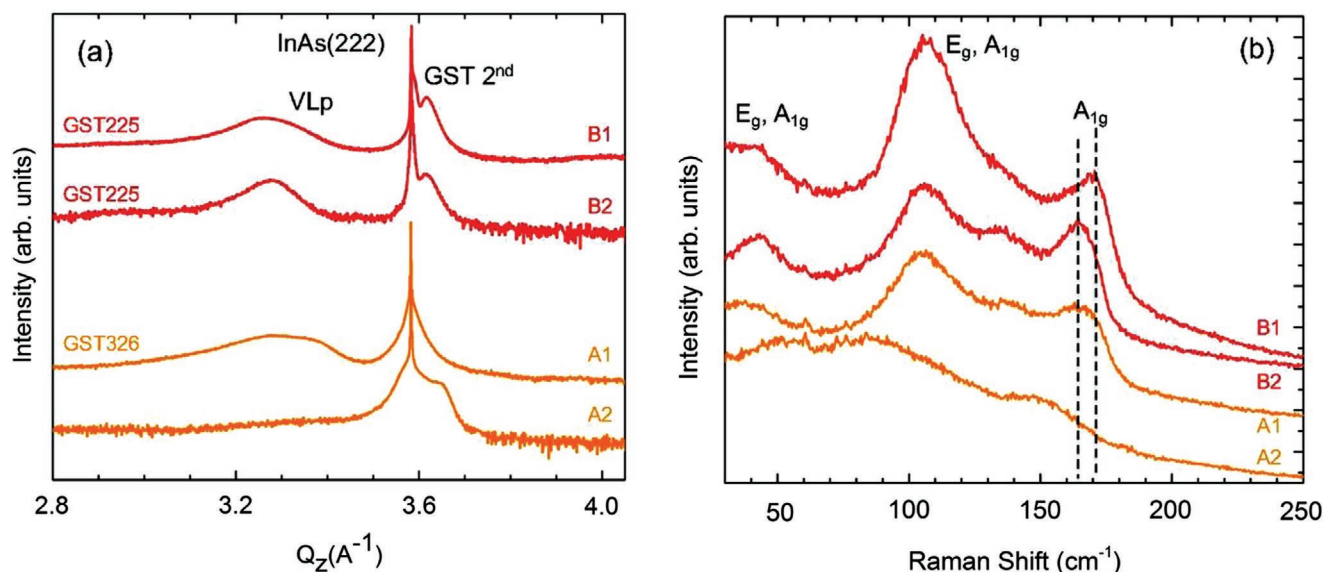
**ADVANCED
SCIENCE NEWS**
www.advancedsciencenews.com

**ADVANCED
MATERIALS
INTERFACES**
www.advmatinterfaces.de

Figure 3. a) Symmetric XRD ω-2θ scans around the second-order InAs and GST reflections for GST/InAs(111)-A and -B samples; b) Raman spectra recorded in backscattering geometry for GST/InAs(111)-A and -B samples (dashed lines are guides to the eye).

is perfectly flat with a self-passivated surface reconstruction. Sample A1, which shows a self-passivated surface reconstruction, is also fully relaxed, while sample A2 exhibiting lower surface quality is only partially relaxed. A pseudomorphic growth is observed for un-passivated surfaces (B2) or rough surfaces (A3, see Supporting Information).

More information on the crystal quality and symmetry of the deposited layers can be obtained by X-ray diffraction (XRD) and Raman spectroscopy. In particular, we can infer the crystal structure (trigonal or cubic) of our GST and the presence of vdW gaps, which can help us to discriminate the kind of epitaxy that occurred. In **Figure 3**a, we present the XRD spectra (symmetric ω-2θ scans along the [111] direction of the substrate) obtained on the different samples (see Table 1). The sharp intense peak at 3.58 Å^{-1} is assigned to the (222) reflection of the InAs substrate. XRD profiles clearly show that all the GST films have a high crystalline order with the out-of-plane orientation along the [111] direction: the peak around 3.62 Å^{-1} represents the second-order GST peak originated from the main Te–Te periodicity, the exact position varying among the samples. Notably, being this interface almost lattice matched, the GST(222) reflection is very close to the InAs(222) reflection. Three out of four samples exhibit a broad peak around 3.3 Å^{-1} that we assign to the first-order satellite peak due to the superstructure originated from the formation of ordered VLs or vdW gaps[31] between GST blocks; the distance between the (222) reflection and the VLs/vdW peaks allows us to determine the block size in the GST sample and the corresponding composition reported in Figure 3. The large width of these peaks is due to the presence of compositional disorder (i.e., the coexistence of GST blocks with different number of layers), quite typical in this kind of alloys.[31] In Figure 3a, we report the composition as determined from the block with the shortest size; in particular samples A1 and B1 show a shoulder at the high Q_z side, which means the presence of a certain percentage of blocks of larger size. The presence of the VL/vdW peak means

that the crystalline structure of such GST films is ordered cubic or trigonal, while sample A2 has a cubic rocksalt structure with no order in the vacancies distribution. From symmetric XRD profiles, we cannot discriminate the crystal symmetry (ordered cubic or trigonal) of GST films; although the out-of-plane lattice parameter of the trigonal phase is expected to be smaller than the cubic one, it varies for different compositions.[43]

To disentangle this point, Raman spectroscopy represents a valuable tool. A superposition of Raman spectra collected on the two sets of samples is shown in Figure 3b. Several modes can be identified, typically assigned to E-like and A-like Raman active modes. E-like modes are related to in-plane displacement patterns of Sb,Te atoms at the vdW gaps, while A-like modes are related to out-of-plane displacement patterns of Sb, Te and Ge atoms at the vdW gaps and inside the blocks.[22,44] In particular, A-like low-frequency and high-frequency modes are extremely sensitive to film ordering and thickness.[22,43] In ref. [43] it has been shown that cubic ordered GST films, where there are not real vdW gaps but not completely depleted VLs, the high energy mode at ≈175 cm^{-1} (related to Te and Sb vibrations at the vdW gaps[22,44]) is strongly reduced with respect to the mode at about 165 cm^{-1} (related to vibrations of Te, Sb and Ge atoms in the blocks[22,44]). By comparing the spectra in Figure 3b, it results that sample B1 is the only one that shows a clear peak at about 175 cm^{-1}, as expected for samples exhibiting completely depleted vdW gaps, sample A1 shows both the features, while in sample B2 the high energy mode is reduced to a faint shoulder. The spectra of sample A2 show almost no first-order Raman modes with very broad features at ≈80 and ≈150 cm^{-1}, as the result of the partial breaking of symmetry in cubic rocksalt due to disorder and defects present in the crystal.[45]

The analysis of the results presented in Figure 3 suggests that flat, 2D substrate surfaces favor the growth of more ordered GST with completely depleted vdW gaps. GST from cubic rocksalt to ordered-cubic to trigonal symmetry is obtained from sample A2 [InAs(111)A surface exhibiting a spotty RHEED

2101556 (4 of 8)

pattern] to sample B1 [best 2D, self-passivated InAs(111)B-2 × 2 surface]. The coexistence of both cubic and trigonal stacking is also possible.[31] These results are in perfect agreement with RSMs: samples A3 (see Supporting Information) and A2 are cubic rocksalt (no VLs/vdW gaps) and they even exhibit pseudomorphic growth or only a partial relaxation. Sample A1 is mixed ordered cubic/trigonal structure and it is completely relaxed, probably exhibiting vdW epitaxy, as sample B1, which is highly ordered (mostly trigonal) and completely relaxed. Sample B2 is practically pseudomorphic, even though we can detect a faint A_{1g}-mode in the Raman spectra that we can ascribe to vibrations at the VLs, therefore with a symmetry at least ordered cubic. This is not surprising as it was deposited on an un-passivated surface and the presence of VLs (which are only partially depleted) cannot be sufficient to relax the lattice parameter. As already noted above, even in the case of sample B1, for which we are observing vdW epitaxy, the relaxation of the lattice parameter is slowing down during the very first stage of the film growth. This behavior can be understood if we consider the fact that a certain degree of compositional disorder is intrinsically present in GST films[31] that can only be partially controlled after a fine-tuning of the growth parameters.[43] As a matter of fact, sample B1 is mainly a mixture of 225 and 326 compositions where each GST block is composed of 9 and 11 layers, respectively (7 layers for GST124).[32] This compositional disorder along the growth direction gives rise, during the coalescence of GST islands, to a possible misalignment of the vdW gaps/VLs as observed in ref. [46]. The formation of lateral bonds, which are stronger than vdW bonds, leads to the formation of stacking faults, which slow down the relaxation process. This result perfectly agrees with the growth of GST on miscut Si substrates where the strain is introduced by lateral bonding at step edges, where the lateral bonding at steps allows the modulation between vdW and classical epitaxy.[16]

In addition, it has been shown that the use of rough InP(111)B substrates reduces or completely suppresses the formation of twins during the epitaxial growth of the topological insulator Bi_2Se_3[23] or that the growth of aligned WSe_2 on sapphire can be guided by step edges.[47] Similarly, this explains the partially relaxed behavior of sample B2, despite the presence of VLs. Our results show that vdW epitaxy of GST can be obtained on InAs(111) substrates provided that the starting surfaces are passivated. Moreover, GST evolves toward a stable structure (trigonal) when the substrate surface is perfectly flat. This interpretation explains the different relaxation behavior observed between the different InAs(111)A, B surfaces studied in this work. In addition, if GST is grown on InAs(001) surface (see Supporting Information of ref. [31]) the film is not textured and crystallographic orientations other than the [00.1] can be found, which means that we can relax completely the need for matching lattice parameter, but not for crystal symmetry.

Table 2 summarizes our former and present results. From the comparison emerges that even under the hypothesis of a mere vdW interaction, as is the case for many of the systems reported, the surface symmetry of the substrate plays an important role in order that vdW epitaxy takes place. For example, it has been demonstrated that graphene, and 2D materials in general, can work as seed layers for vdW epitaxy.[8–10] The so-called wetting transparency of graphene allows also for the remote epitaxy of GaAs on GaAs enabling the possibility to grow removable semiconductor layers.[11] This means that the vdW potentials of graphene can be so weak to be unable to screen the surface potential of a substrate below the graphene. We can infer that the same may hold for the very surface layer of many passivated surface reconstructions. This means that, even in presence of a pure vdW epitaxy, the substrate surface orientation always influences the symmetry of the growing film. This picture is consistent with a model proposed in ref. [12], where the authors state that the vdW epitaxy can be obtained when the symmetry group of the substrate is a subgroup of that of the 2D material. Actually, for all the cases reported in Table 2, the substrate orientation is always cubic (111) or has an in-plane hexagonal symmetry, but the vdW epitaxy is observed only on passivated covalent surfaces (or in the presence of a graphene buffer layer). Epitaxy on un-passivated covalent surfaces increases drastically the interaction with the substrate leading to the formation of coincidence lattices or to a partially relaxed growth. Coincidence lattice is incompatible with pure vdW epitaxy,[6] as its observation indicates the presence of bonds between the substrate and the epilayer. However, even for the passivated surfaces (SiC-6√3×6√3R30° buffer layer, last row in Table 2[9]), lattice matching can still play a role in the formation of coincidence lattices. This means that the local distribution of surface potential can lead to the natural formation of coincidence lattices and must be considered in the search for suitable systems for vdW epitaxy. Thus, the presence of a coincidence lattice can occur for both vdW and classical epitaxy. Finally, epitaxial growth on substrates with a rough surface or significant miscut increases the substrate–film interaction even further. This can be used to stabilize the cubic phase of GST or prevent twinning.

To fully understand the difference between epitaxy performed on passivated covalent and weakly interacting 2D surfaces, such as graphene, we focus our attention on the formation of twist and twin domains (last two columns of Table 2). Both are typical for the epitaxial growth of 2D materials and can be attributed to the weak interaction across the interface with the substrate or between vdW blocks. In the case of vdW epitaxy on pure 2D material substrates, both twins and twists are observed as expected, whereas if vdW epitaxy is performed on passivated covalent surfaces twists are suppressed.[33] This is an indication of a stronger interaction with the underlying substrate. This form of vdW epitaxy provides the striking advantage of offering an epitaxial registry that facilitates the growth of single crystals with the full freedom of epilayer relaxation. Furthermore, by adopting a passivated substrate with miscut, also twins are nearly suppressed, and a certain degree of strain engineering is allowed.[16] Table 2 provides a valuable toolbox to help anticipate vdW epitaxy of such unconventional heterostructures, allowing practical exploitation in large-scale monolithical material synthesis with high crystalline quality.

3. Conclusions

In conclusion, we have presented evidence of the key role played by the substrate surface in vdW epitaxy. Substrate symmetry influences the symmetry of the growing film and, for

Table 2. Summary of former[9,16,33] and present results on the growth of GST and Sb₂Te₃ films on passivated, non-passivated covalent substrates and 2D substrates under high and low mismatch conditions.

	Substrate Surface Structure				Epitaxy	GST Crystal Structure	Twists	Twins
High Mismatch GST/Si(111) Sb₂Te₃/Si(111)	**Passivated**	Sb-√3×√3R30°	Miscut	0.03°	vdW		**No**	Yes
				3° (only for GST)	mixed classical/vdW	Trigonal	No	No
				4°	mixed classical/vdW	Trigonal	No	No
				6°	mixed classical/vdW	Trigonal	No	No
		H-1×1			vdW		**No**	Yes
	Not Passivated and/or defective structure	7×7			Coincidence lattice		Yes	Yes
		Sb-5√3×5√3R30°			Coincidence lattice		Yes	Yes
Low Mismatch GST/InAs(111)	**Passivated**	(111)A-2×2			vdW	Trigonal	**No**	Yes
		(111)B-2×2			vdW	Trigonal	**No**	Yes
	Not Passivated and/or defective structure	(111)B-1×1			partially relaxed	Ordered Cubic	No	Yes
		(111)A,B - 3D rough surface			partially relaxed	Cubic	No	Yes
vdW Substrate Sb₂Te₃/Graphene	epitaxial monolayer **Graphene**/SiC-6√3×6√3R30°				vdW		**Yes**	**Yes**
	quasi freestanding bilayer **Graphene**/oxidized SiC				vdW		**Yes**	**Yes**
	SiC-6√3×6√3R30° buffer layer – passivated surface				Coincidence lattice		Yes	Yes

extremely well passivated covalent or pure 2D surfaces, vdW epitaxy can be fully achieved. When this requirement is relaxed, an interaction with the substrate surface arises, which can lead to the formation of coincidence lattices or induce a partially relaxed growth. The latter type of epitaxy provides the advantage of offering an epitaxial registry similar to the well-known epitaxial classical cases. Indeed, it might facilitate the growth of single crystals with the full freedom of epilayer relaxation. Furthermore, adopting a passivated substrate with miscut, strain engineering is allowed. All this information provides a toolbox to predict epitaxial growth rules and to allow large-scale monolithical material synthesis for the exploitation of unconventional device designs.

4. Experimental Section

Sample Preparation: InAs(111)A-2 × 2 surfaces were prepared by annealing at 400 °C epiready wafers in ultra-high vacuum (UHV) in the MBE system dedicated to GST growth. Depending on the time of annealing the RHEED pattern quickly deteriorates from quite streaky (sample A1) to spotty (sample A2), see Table 1 and Figure S1 in Supporting Information. InAs(111)B-2 × 2 and −1 × 1 surfaces were

obtained by annealing at 260 °C, in the MBE system dedicated to GST growth, As-capped epitaxial InAs(111)B films grown in a separate MBE system (Table 1 and Figure S1 in Supporting Information).

MBE growth of epitaxial GST (with thicknesses ranging from 24 to 28 nm) was performed on InAs(111)A-2 × 2, InAs(111)B-2 × 2 and InAs(111)B-1 × 1 surfaces. The deposition of the $(GeTe)_m(Sb_2Te_3)_n$ alloys was performed for substrate temperatures in the range 200–250 °C. Flux ratios between the elemental sources of the GST were properly chosen in order to obtain GST layers with the main composition $Ge_2Sb_2Te_5$.[43]

XRD Characterization: Samples were characterized by means of ex-situ XRD, utilizing a PANalytical X'Pert Pro Materials Research diffractometer equipped with a Ge (220) hybrid monochromator and Cu Kα_1 ($\lambda = 1.540598$ Å) X-ray radiation. radiation ($\lambda = 1.540598$ Å). Specular ω-2θ scans were performed in double axes mode in order to access the growth direction of the films, in a range of 10°–110°, with a step 0.02° and integration time of 2.5 s. RSMs were performed around the asymmetric InAs(224) Bragg reflection in coplanar configuration.

Raman Characterization: Spectra were acquired exciting samples with the 632.8 nm line of a He–Ne laser and the scattered light was analyzed using a spectrometer equipped with an LN_2-cooled charge-coupled device detector. The spectra were recorded in backscattering geometry in crossed and parallel polarization configurations. The emission was focused by a microscope objective with 0.9 numerical aperture and the same objective was used for the collection of the signal. The spectral resolution achieved is 0.7 cm⁻¹ and a notch filter suppressed the stray light.

Supporting Information

Supporting Information is available from the Wiley Online Library or from the author.

Conflict of Interest

The authors declare no conflict of interest.

Author Contributions

Samples were grown by F.A., V.B. and J.E.B.. F.A., J.E.B, and S.C. performed XRD, and E.Z. Raman characterization. F.A. performed data analysis. R.C., E.Z. and S.C. contributed to the interpretation of the results. The paper was written by F.A. and R.C. with the help and through contributions from all co-authors. All authors have given approval to the final version of the manuscript. The project was initiated and conceptualized by F.A. and R.C.

Data Availability Statement

The data that support the findings of this study are available from the corresponding author upon reasonable request.

[1] A. K. Geim, I. V. Grigorieva, *Nature* **2013**, *499*, 419.
[2] Y. Liu, N. O. Weiss, X. Duan, H.-C. Cheng, Y. Huang, D. Xiangfeng, *Nat. Rev. Mater.* **2016**, *490*, 16042.
[3] K. S. Novoselov, A. Mishchenko, A. Carvalho, A. H. Castro Neto, *Science.* **2016**, *353*, aac9439.
[4] J. R. Schaibley, H. Yu, G. Clark, P. Rivera, J. S. Ross, K. L. Seyler, W. Yao, X. Xu, *Nat. Rev. Mater.* **2016**, *1*, 16055.
[5] D. Akinwande, C. Huyghebaert, C.-H. Wang, M. I. Serna, S. Goossens, L.-J. Li, H.-S. P. Wong, F. H. L. Koppens, *Nature* **2019**, *573*, 507.
[6] A. Koma, K. Sunouchi, T. Miyajima, *Microelectron. Eng.* **1984**, *2*, 129.
[7] W. Mortelmans, S. De Gendt, M. Heyns, C. Merckling, *Appl. Mater. Today* **2021**, *22*, 100975.
[8] K. Chung, C.-H. Lee, G.-C. Yi, *Science.* **2010**, *330*, 655.
[9] J. E. Boschker, L. A. Galves, T. Flissikowski, J. M. J. Lopes, H. Riechert, R. Calarco, *Sci. Rep.* **2015**, *5*, 18079.
[10] J. Y. Park, G.-H. Lee, J. Jo, A. K. Cheng, H. Yoon, K. Watanabe, T. Taniguchi, M. Kim, P. Kim, G.-C. Yi, *2D Mater.* **2016**, *3*, 035029.
[11] Y. Kim, S. S. Cruz, K. Lee, B. O. Alawode, C. Choi, Y. Song, J. M. Johnson, C. Heidelberger, W. Kong, S. Choi, K. Qiao, I. Almansouri, E. A. Fitzgerald, J. Kong, A. M. Kolpak, J. Hwang, J. Kim, *Nature* **2017**, *544*, 340.
[12] J. Dong, L. Zhang, X. Dai, F. Ding, *Nat. Commun.* **2020**, *11*.
[13] M. Heilmann, M. Bashouti, H. Riechert, J. M. J. Lopes, *2D Mater.* **2018**, *5*, 025004.
[14] X. Zhang, F. Zhang, Y. Wang, D. S. Schulman, T. Zhang, A. Bansal, N. Alem, S. Das, V. H. Crespi, M. Terrones, J. M. Redwing, *ACS Nano* **2019**, *13*, 3341.
[15] W. Mortelmans, K. De Smet, R. Meng, M. Houssa, S. De Gendt, M. Heyns, C. Merckling, *Adv. Mater. Interfaces* **2021**, *8*, 2100438.
[16] E. Zallo, S. Cecchi, J. E. Boschker, A. M. Mio, F. Arciprete, S. Privitera, R. Calarco, *Sci. Rep.* **2017**, *7*, 1466.
[17] R. Wang, F. R. L. Lange, S. Cecchi, M. Hanke, M. Wuttig, R. Calarco, *Adv. Funct. Mater.* **2018**, *28*, 1705901.
[18] P. A. Vermeulen, J. Mulder, J. Momand, B. J. Kooi, *Nanoscale* **2018**, *10*, 1474.
[19] W. Mortelmans, W. Mortelmans, A. Nalin Mehta, A. Nalin Mehta, Y. Balaji, Y. Balaji, S. Sergeant, R. Meng, M. Houssa, S. De Gendt, S. De Gendt, M. Heyns, M. Heyns, C. Merckling, *ACS Appl. Mater. Interfaces* **2020**, *12*, 27508.
[20] S. Cecchi, E. Zallo, J. Momand, R. Wang, B. J. Kooi, M. A. Verheijen, R. Calarco, *APL Mater.* **2017**, *5*, 026107.
[21] S. Cecchi, D. Dragoni, D. Kriegner, E. Tisbi, E. Zallo, F. Arciprete, V. Holý, M. Bernasconi, R. Calarco, *Adv. Funct. Mater.* **2019**, *29*, 1805184.
[22] E. Zallo, D. Dragoni, Y. Zaytseva, S. Cecchi, N. I. Borgardt, M. Bernasconi, R. Calarco, *Phys Status Solidi Rapid Res Lett* **2021**, *15*, 2000434.
[23] N. V. Tarakina, S. Schreyeck, M. Luysberg, S. Grauer, C. Schumacher, G. Karczewski, K. Brunner, C. Gould, H. Buhmann, R. E. Dunin-Borkowski, L. W. Molenkamp, *Adv. Mater. Interfaces* **2014**, *1*, 1400134.
[24] C. W. Liu, J. J. Dai, S. K. Wu, N. Q. Diep, S. H. Huynh, T. T. Mai, H. C. Wen, C. T. Yuan, W. C. Chou, J. L. Shen, H. H. Luc, *Sci. Rep.* **2020**, *10*, 12972.
[25] M. Wuttig, N. Yamada, *Nat. Mater.* **2007**, *6*, 824.
[26] Intel Optane Technology, see https://www.intel.com/content/www/us/en/architecture-and-technology/intel-optane-technology.html for for combi- nation of *3D XPointTM memory media, Intel Memory and Storage Controllers, Intel Interconnect IP and IntelVR softw* **2017**.
[27] M. Technology, see https://www.micron.com/products/advanced-solutions/3d-Xpoint-Technology for 3D XPointTM Memory technology, an entirely new class of nonvolatile memory **2016**.
[28] A. Sebastian, M. L.e Gallo, R. Khaddam-Aljameh, E. Eleftheriou, *Nat. Nanotechnol.* **2020**, *15*, 529.
[29] W. Zhang, R. Mazzarello, M. Wuttig, E. Ma, *Nat. Rev. Mater.* **2019**, *4*, 150.
[30] K. Ding, J. Wang, Y. Zhou, H. Tian, L. Lu, R. Mazzarello, C. Jia, W. Zhang, F. Rao, E. Ma, *Science.* **2019**, *366*, 210.
[31] V. Bragaglia, F. Arciprete, W. Zhang, A. M. Mio, E. Zallo, K. Perumal, A. Giussani, S. Cecchi, J. E. Boschker, H. Riechert, S. Privitera, E. Rimini, R. Mazzarello, R. Calarco, *Sci. Rep.* **2016**, *6*, 23843.
[32] J. L. F. Da Silva, A. Walsh, H. Lee, *Phys. Rev. B Condens. Matter Mater. Phys.* **2008**, *78*, 224111.
[33] J. E. Boschker, J. Momand, V. Bragaglia, R. Wang, K. Perumal, A. Giussani, B. J. Kooi, H. Riechert, R. Calarco, *Nano Lett.* **2014**, *14*, 3534.
[34] P. Tsipas, D. Tsoutsou, S. Fragkos, R. Sant, C. Alvarez, H. Okuno, G. Renaud, R. Alcotte, T. Baron, A. Dimoulas, *ACS Nano* **2018**, *12*, 1696.
[35] A. Ohtake, Y. Sakuma, *J. Phys. Chem. C* **2020**, *124*, 5196.

[36] J. E. Boschker, M. Boniardi, A. Redaelli, H. Riechert, R. Calarco, *Appl. Phys. Lett.* **2015**, *106*, 023117.

[37] M. Boniardi, J. E. Boschker, J. Momand, B. J. Kooi, A. Redaelli, R. Calarco, *Phys Status Solidi Rapid Res Lett* **2019**, *13*, 1800634.

[38] A. Taguchi, K. Kanisawa, *Appl. Surf. Sci.* **2006**, *252*, 5263.

[39] J. Yang, C. Nacci, J. Martínez-Blanco, K. Kanisawa, S. Fölsch, *J. Phys. Condens. Matter* **2012**, *24*, 354008.

[40] E. Hilner, E. Lundgren, A. Mikkelsen, *Surf. Sci.* **2010**, *604*, 354.

[41] A. Taguchi, *J. Cryst. Growth* **2005**, *278*, 468.

[42] O. E. Tereshchenko, D. Paget, A. C. H. Rowe, V. L. Berkovits, P. Chiaradia, B. P. Doyle, S. Nannarone, *Surf. Sci.* **2009**, *603*, 518.

[43] V. Bragaglia, F. Arciprete, A. M. A. M. Mio, R. Calarco, *J. Appl. Phys.* **2018**, *123*, 215304.

[44] G. C. Sosso, S. Caravati, C. Gatti, S. Assoni, M. Bernasconi, *J. Phys. Condens. Matter* **2009**, *21*, 245401.

[45] V. Bragaglia, K. Holldack, J. E. Boschker, E. Zallo, F. Arciprete, T. Flissikowski, R. Calarco, *Sci. Rep.* **2016**, *6*, 28560.

[46] J. Momand, F. R. L. Lange, R. Wang, J. E. Boschker, M. A. Verheijen, R. Calarco, M. Wuttig, B. J. Kooi, *J. Mater. Res.* **2016**, *31*, 3115.

[47] L. Chen, B. Liu, M. Ge, Y. Ma, A. N. Abbas, C. Zhou, *ACS Nano* **2015**, *9*, 8368.

2101556 (8 of 8)